Available online at www.sciencedirect.com
ScienceDirect
Russian Geology and Geophysics 49 (2008) 790–802
RUSSIAN GEOLOGY AND GEOPHYSICS
www.elsevier.com/locate/rgg

Improving inversion quality for IP-affected TDEM data

E.Yu. Antonov * and A.N. Shein

Trofimuk Institute of Petroleum Geology and Geophysics, Siberian Branch of the RAS, 3 prosp. Akad. Koptyuga, Novosibirsk, 630090, Russia

Received 19 July 2007; accepted 31 January 2008
Available online xx September 2008

Abstract

We suggest new inversion techniques for IP-affected TDEM data. The method implies joint inversion of inductive and galvanic measurements, the galvanic array being configured in a way to separate the polarization and induction components of transient responses from a layered polarizable earth. The IP effects turned out to be reducible at a certain receiver configuration, which was predicted theoretically and proved valid in field tests.
© 2008, IGM SB RAS. Published by Elsevier B.V. All rights reserved.

Keywords: Induced polarization (IP); time-domain electromagnetic (TDEM) method; forward modeling and inversion

Introduction

Galvanic TDEM responses often bear an induced polarization (IP) component. Historically, it was the use of galvanic measurement systems that gave rise to the IP method which demonstrated its high efficiency in resistivity surveys for mineral prospecting and structural applications. Induced polarization is a complex phenomenon controlled by many physical and physicochemical reactions associated with passage of current through rocks. IP effects have been described on microscopic and macroscopic scales in numerous models. In the Russian literature they are, for instance, a macroscopic cell model of a uniform ion-polarizable conductor (Postel'nikov, 1964), a model of interfacial polarization in a layered half-space of alternating thin conductive and resistive beds (Maxwell-Wagner effect) (Gubatenko, 1991). We may also cite treatises by Gennadinik (1967), Sheinmann (1969), Komarov (1972), and Kormil'tsev (1980) as an important contribution to the IP theory. Most IP models stem from a phenomenological approach implying boundary-value solutions of Maxwell's equations for frequency-dependent resistivity, with the Cole-Cole formula applied commonly to account for polarization effects:

$$\rho(\omega) = \rho_0\left[1 - \eta\left(1 - \frac{1}{1 + (i\omega\tau)^c}\right)\right] \quad (1)$$

for resistivity (Pelton et al., 1978) and

$$\sigma(\omega) = \sigma_0 \frac{1 + (-i\omega\tau)^c}{1 + (1 - \eta)(-i\omega\tau)^c} \quad (2)$$

for conductivity (Lee, 1981), where η is chargeability (ρ_0 and σ_0 are, respectively, the high-frequency dc resistivity and the conductivity), τ is the relaxation time, and c is the exponent describing the variation of phase with frequency.

Equations (1) and (2) are good for forward modeling of TEM responses of a polarizable earth but inversion is often difficult as the number of unknowns may be too large. Inversion for an n-layer half-space requires solutions with $(2n - 1)$ unknowns $[\rho_{0,1}, h_1, ..., \rho_{0,n-1}, h_{n-1}, \rho_{0,n}]$ for nonpolarizable earth and $(5n - 1)$ unknowns $[\rho_{0,1}, \eta_1, \tau_1, c_1, h_1, ..., \rho_{0,n-1}, \eta_{n-1}, \tau_{n-1}, c_{n-1}, h_{n-1}, \rho_{0,n}, \eta_n, \tau_n, c_n]$ for a polarizable case, where h is the layer thickness. Thus, one needs an inversion algorithm in which to separate the search of model parameters for the basic nonpolarizable section $[\rho_{0,1}, h_1, ..., \rho_{0,n-1}, h_{n-1}, \rho_{0,n}]$ and the Cole-Cole parameters $[\eta_1, \tau_1, c_1, ..., \eta_n, \tau_n, c_n]$.

This separation is somehow achieved in differential-normalized resistivity (DNR) surveys based on the idea that late-time responses of a nonpolarizable layered earth are independent of array spacing while the inductive component is damped and the polarization component is amplified in the differential (spatially-differentiated) signal (Davydycheva et al., 2006; Legeido et al., 1990; Mandel'baum et al., 1988; Rykhlinskii et al., 1970). However, a shortcoming of the DNR method is that it additionally uses logging or other methods to gain a priori data providing an appropriate approximation

* Corresponding author.
E-mail address: antonovey@ipgg.nsc.ru (E.Yu. Antonov)

of the nonpolarizable conductor in the starting model, necessary for successful processing of IP-affected TEM transients.

We suggest measurement techniques in which the signal is decomposed into the inductive and polarization components using special galvanic system configurations or induction data.

Forward modeling of finite-size array transient responses

We begin with a brief description of forward algorithms and numerical experiments, which appears pertinent as forward modeling is an essential tool in our study. Finite-size array responses are found as horizontal electric dipole solutions by integration over the system of point electric sources along the transmitter line and dipoles along the receiver line. This approach is also fit for inductive measurement systems which are simulated in a computationally efficient way as electric dipoles along loops. Let a layered half-space have the resistivities $\rho_1, ..., \rho_i, ..., \rho_n$, the magnetic permeabilities $\mu_1, ..., \mu_i, ..., \mu_n$, and the depths of the layer boundaries $z_1, ..., z_I, ..., z_n$, with the z axis in the Cartesian coordinates directed downward. The TEM field arising on the removal of the transmitter current in a horizontal electric dipole $I_x dl$ oriented along the x axis, ($E_\parallel$ and $E_\perp$, parallel and orthogonal to the transmitter) is (Tabarovskii, 1975):

$$E_\parallel(t) = -\frac{I_x\, dl\rho_1}{\pi^2}\int_{-\infty}^{\infty}\frac{e^{-i\omega t}}{-i\omega}\left\{\int_0^\infty\left[f^E_{zz_0}\frac{\partial^2 J_0(u\,|r-r_0|)}{\partial x^2} - k_1^2 f^H \frac{\partial^2 J_0(u\,|r-r_0|)}{\partial y^2}\right]u\,du\right\}d\omega. \quad (3)$$

$$E_\perp(t) = -\frac{I_x\, dl\rho_1}{\pi^2}\int_{-\infty}^{\infty}\frac{e^{-i\omega t}}{-i\omega}\left\{\int_0^\infty\left[f^E_{zz_0}\frac{\partial^2 J_0(u\,|r-r_0|)}{\partial x\partial y} - k_1^2 f^H \frac{\partial^2 J_0(u\,|r-r_0|)}{\partial x\partial y}\right]u\,du\right\}d\omega. \quad (4)$$

where $I_x dl$ is the dipole moment, (r_0, z_0) and (r, z) are the cylindrical coordinates of the transmitter and receiver, respectively (the Cartesian and cylindrical coordinates have the same origin), $u = \sqrt{k_x^2 + k_y^2}$, where k_x and k_y are the coordinates of the Fourier images along the x and y axes, and J_0 is the zero-order Bessel function of the first kind. The integrand functions $f^E(u, \omega, z, z_0)$ and $f^H(u, \omega, z, z_0)$ define the field dependence on earth's resistivity and magnetic permeability, on the interface depths ($z_1, z_2, ..., z_{n-1}$), on the transmitter and receiver depths z_0 and z, and on the frequency ω; the superscripts $\Phi = \{E \vee H\}$ denote the electric or magnetic mode, respectively. The array geometry is taken into account in the Bessel function argument.

The functions $f^\Phi(u, \omega, z, z_0)$ are calculated using recurrent formulas from (Tabarovskii, 1979):

$$\alpha_n^\Phi = 0,$$

$$\beta_{j-1}^\Phi = \frac{\gamma_j^\Phi}{\gamma_{j-1}^\varphi}\frac{p_{j-1}}{p_j}\frac{\alpha_j^\Phi + 1}{\alpha_j^\Phi - 1},$$

$$R_{j-1}^\Phi = \frac{1+\beta_{j-1}^\Phi}{1-\beta_{j-1}^\Phi},$$

$$\alpha_{j-1}^\Phi = -e^{-2p_{j-1}(z_{j-1}-z_{j-2})}R_{j-1}^\Phi,$$

where $j = 1, ..., 2$, $p_j = \sqrt{u^2 + k_j^2}$, $k_j^2 = -i\omega\mu_j/\rho_j$, $\rho_j = \rho_j(\omega)$ is the complex resistivity governed by (1), μ_1 is the magnetic permeability, and $\gamma_j^\Phi = \begin{cases} 1/\rho_j, & \Phi = E \\ \mu_j, & \Phi = H \end{cases}$. Once R_1^Φ have been obtained using these equations, the functions $f^\Phi(u, \omega, z, z_0)$ are found as $f^\Phi(u, \omega, z, z_0) = -\frac{e^{-p_1(2z_1+z_0-z)}}{2p_1}R_1^\Phi + \frac{e^{-p_1|z-z_0|}}{2p_1}$.

The inner integrals along the spatial frequency u in (3) and (4), which is the Hankel transform, are calculated using special spline interpolation quadratures based on the Laguerre polynomials. The quadrature coefficients for point sources are found once and saved in a special file. To simulate a finite-size system, one just has to integrate the quadratures along the transmitter and receiver coordinates. This approach allows fast computing for measurement systems of an arbitrary geometry.

We report modeling results obtained with the **<FwPr_LL>** (for galvanic arrays) and **<Unv_QQ>** (for inductive arrays) software*.

Inversion

Inversion was applied to

— compare inductive and galvanic data processing (programs **<Inv_QQ>***, **<Inv_LL>***);

— find the optimal receiver position where IP effects in transients are the weakest (program **<InvFI_LL>***).

The half-space parameters were found by minimization of the residual functional which is the weighted rms error (misfit between the measured and computed data). The goal function was specified as

$$\Phi(\mathbf{P}, t) = \left[\frac{1}{N-1}\sum_{j=1}^{N}\left(\frac{f^e(t_i) - f^i(\mathbf{P}, t_i)}{\delta(t_i) f^e(t_i)}\right)^2\right]^{1/2}, \quad (5)$$

where is the vector from the space of model parameters, $\{t_I, i = 1, ..., N\}$ are the delay times, $f^e(t)$ is the measured signal, $f^t(\mathbf{P}, t)$ is the computed signal, and δ is the relative measurement error. Minimization was performed by fitting the model parameters (**P**), following the methods of Nelder and Mead (1965) and Gill et al. (1981). This inversion technique is advantageous over the gradient methods as it does not require derivative forward solutions for the model parameters. The application of the deformed polyhedron method to inversion

* Original software designed by E.Yu. Antonov, at Trofimuk Institute of Petroleum Geology and Geophysics, Novosibirsk.

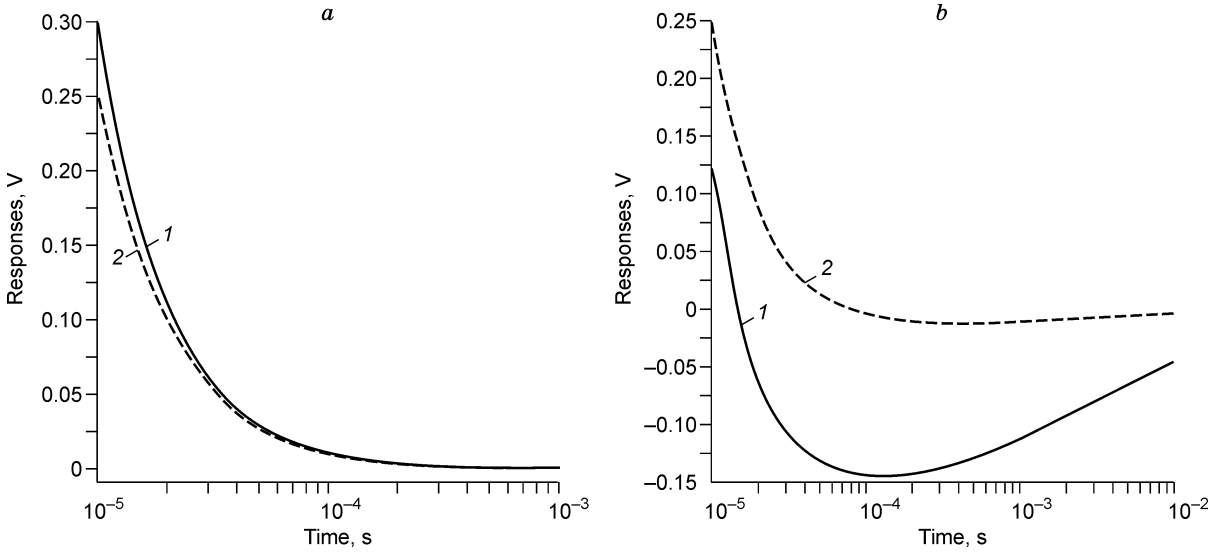

Fig. 1. Influence of array geometry on transient responses. *1* — dipole, *2* — line, *a* — nonpolarizable conductor: ρ = 100 Ohm·m; *b* — polarizable conductor, ρ = 100 Ohm·m, η = 0.05, τ = 0.01 s, *c* = 0.5.

of IP-affected TEM data is discussed in (Epov et al., 2006; Kozhevnikov and Antonov, 2006, 2007; Nevedrova and Antonov, 2004; Yeltsov et al., 1999, 2002).

Simulating transient responses of a polarizable earth

According to Sheinmann (1969), no special tools are needed to calculate alternating fields of frequency-dependent two-phase (TP) media*. The same holds on the passage from alternating to transient fields. Difficulties arise only in the transformation and calculation of integrals: Transient responses, even in the simplest frequency-dependence cases, have no analytical expression, and all solutions have to be numerical. Thus, simulating the responses of media with complex frequency-dependent resistivity, magnetic permeability, and electric permittivity has become a special line of research through the recent decades. It differs from other modeling methods as it has to account for the size and configuration of measurement systems, which reduces the applicability of the dipole approximation. In the case of nonpolarizable conductors, due regard for the array size is essential at early times and the dipole approximation becomes appropriate at later times. The IP-affected transients, however, depend on the system size at all delay times. Figure 1 shows responses of a nonpolarizable (*a*) and a polarizable (*b*) earth both in the dipole approximation and with regard to the array size, for a model with the resistivity ρ = 100 Ohm·m, the chargeability η = 0.05, τ = 0.01 s, and the exponent *c* = 0.5, typical of the Novosibirsk area. Simulated were equatorial galvanic array transients, with a current-electrode separation of AB = 100 m, a potential-electrode separation of MN = 50 m, and an array spacing (distance between line centers) of *r* = 50 m.

Unlike the responses of a nonpolarizable earth, the polarizable conductor responses are highly sensitive to the duration of the transmitter current. This may provide useful additional information because effects from even short current pulses become measurable due to a slow decay of the field. See Fig. 2 for measured (*a*) and synthetic (*b*) equatorial-array responses and synthetic loop responses (*c*) of a polarizable earth (ρ = 100 Ohm·m, η = 0.05, τ = 0.01 s, *c* = 0.5) to current pulses of different durations (3, 10, and 30 ms, respectively). The changes in current duration, which is a controllable parameter of excitation, produce curve families (Fig. 2) of a particular pattern (e.g., sign reversal vicinity) which may be useful in joint inversion.

Inductive and galvanic measurements in a polarizable earth: comparison of results

Inductive and galvanic measurement systems differ in sensitivity to IP effects. Inductive measurement and excitation is less efficient at relaxation times more than 0.1 ms. The reason is that the primary vortex field from an ungrounded transmitter is too short to polarize the earth while direct current in an electric line can induce processes decaying much more slowly than the transient process due uniquely to conduction.

This difference between the two methods can be employed to improve the processing quality for IP-affected galvanic data. Here are some examples of inductive and galvanic data processing (Fig. 3), with reference models typical of the Transbaikalia and Siberian craton areas (East Siberia) obtained from DNR surveys by people from the Siberian Research and Development Company (Irkutsk). Compared are the responses of nonpolarizable (models 1a, 2a) and polarizable (models 1b, 2b) conductors (see Tables 1 and 2 for the model parameters).

* As in a two-phase solid-liquid model of rocks, in which the liquid is an aqueous solution of an electrolyte (Sheinman, 1969).

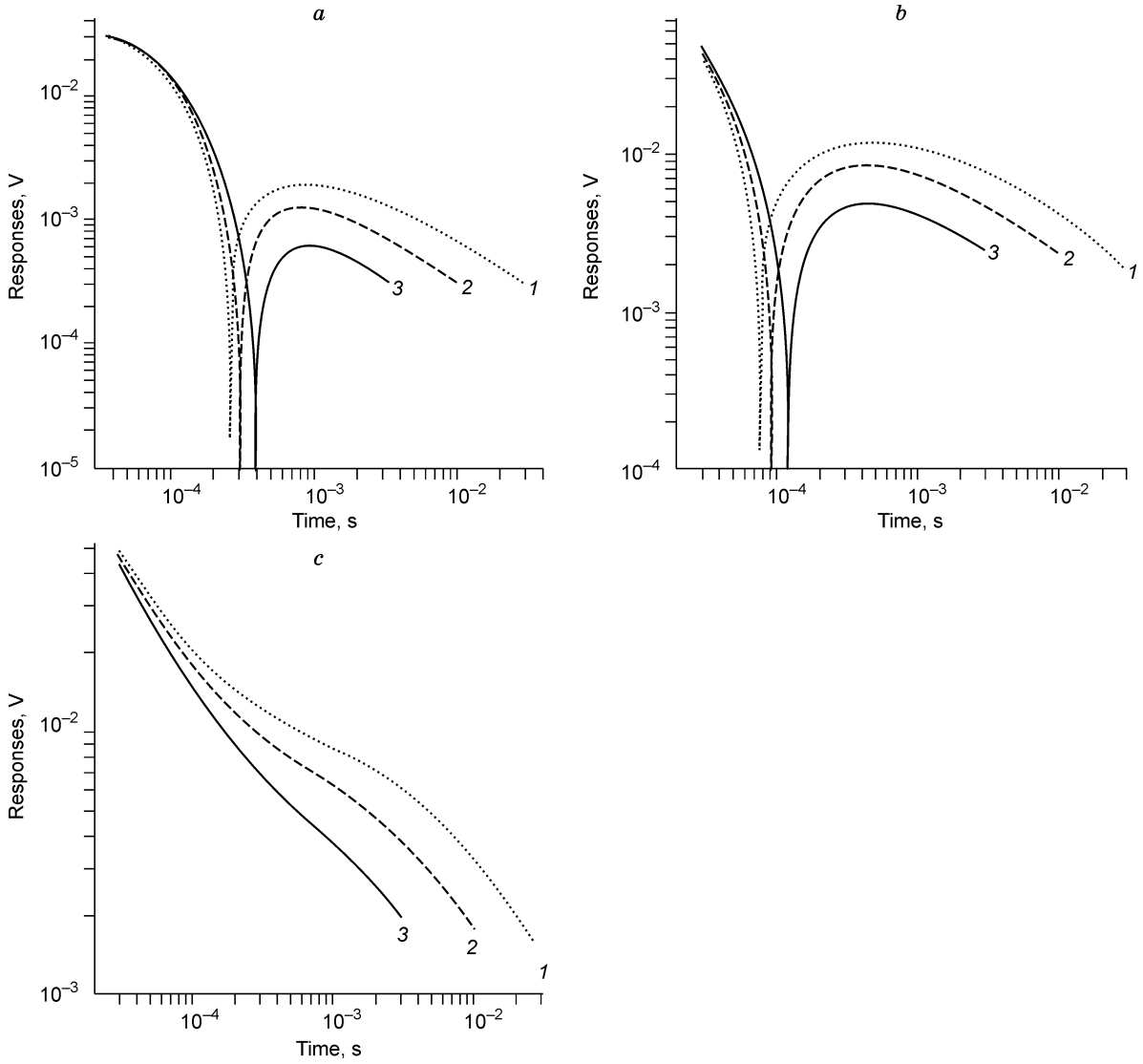

Fig. 2. Transient responses of a polarizable earth (ρ = 100 Ohm·m, η = 0.05, τ = 0.01 s, *c* = 0.5) at different durations of current pulses: *1* — 30, *2* — 10; *3* — 3 ms. *a* — field equatorial array (*r* = 25 m, φ = 90°), *b* — synthetic equatorial array (*r* = 25 m, φ = 90°), *c* — synthetic parallel array (*r* = 100 m, φ = 0°).

The two measurement systems were as follows: coincident loops (500×500 m), equatorial galvanic array (transmitter line of AB = 500 m and receiver line of MN = 250 m, *r* = 250 m, angle from **AB** to **r** φ = 90°).

In model 1 (Transbaikalia), the inductive component is weakly affected by IP (Fig. 3, *a*), which corresponds to the case of a nonpolarizable earth (model 1a).

Model 2 (an area of the Krasnoyarsk Territory) is more complicated because of IP effects after 50 ms in the computed inductive response. Processing these IP-affected data with a starting model of a nonpolarizable layered conductor can give a false insulator (Fig. 3, *b*). To avoid mistakes of this kind, one has to reduce the time window used in inversion. IP effects in inductive data can be often identified from the behavior of the apparent resistivity transformant, for instance, from a steep slope of the right-hand branch (in addition to the subsurface heterogeneity). The examples of two-component measurements prompt that stepwise inversion may be reasonable in this case, with estimating the resistivity and layer thicknesses of a nonpolarizable conductor from inductive data at the first step and the Cole-Cole (*m*, τ, and *c*) inversion of galvanic data at the second step.

Azimuth dependence of parallel galvanic responses

In this section we discuss the behavior of the transient electric field and the way to minimize the polarization component by configuring a parallel HEL (horizontal electric line) galvanic array. In the measurement system choice we proceeded from potentialities of frequency-domain EM systems to detect polarization effects (Hohmann et al., 1970) and from our modeling results for horizontal electric and all magnetic components excited by an electric line in a polarizable earth. The modeling was applied to estimate the IP sensitivity of each constituent vector of the electric and

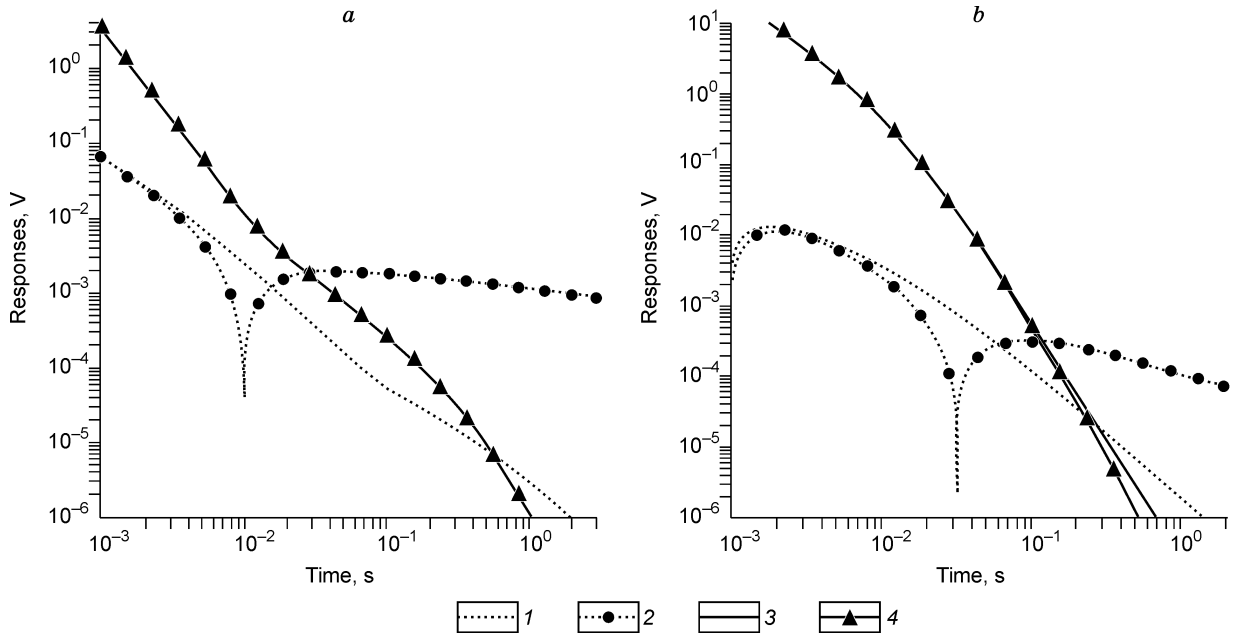

Fig. 3. Inversion results for IP-free (*1*) and IP-affected (*2*) galvanic array and IP-free (*3*) and IP-affected (*4*) inductive array data. *a* — model 1, Table 1; *b* — model 2, Table 2.

Table 1
DNR data from Transbaikalia

Model 1a			Model 1b				
Layer	ρ, Ohm·m	*h*, m	ρ, Ohm·m	*h*, m	η	τ, s	*c*
1	107	100	107	100	0.01	0.1	0.07
2	122	90	122	90	0.01	0.2	0.64
3	168	330	168	330	0.024	0.27	0.35
4	94	305	94	305	0.005	0.8	0.4
5	115	300	115	300	0.004	0.8	0.2
6	11	1250	11	1250	—	—	—
7	1000	∞	1000	∞	—	—	—

Table 2
DNR data from Krasnoyarsk Territory

Model 2a			Model 2b				
Layer	ρ, Ohm·m	*h*, m	ρ, Ohm·m	*h*, m	η	τ, s	*c*
1	3.9	34	3.9	34	0.026	0.04	0.65
2	420	73	420	73	0.026	0.25	0.45
3	7.8	180	7.8	180	0,02	0.01	0.67
4	80	220	80	220	0.01	0.01	0.5
5	280	300	280	300	0.018	0.01	0.5
6	8000	80	8000	80	0.13	0.01	0.5
7	45	580	45	580	0.01	0.1	0.5
8	350	940	350	940	0.01	0.1	0.5
9	30	50	30	50	0.01	0.1	0.5
10	1000	∞	1000	∞	0.01	0.1	0.5

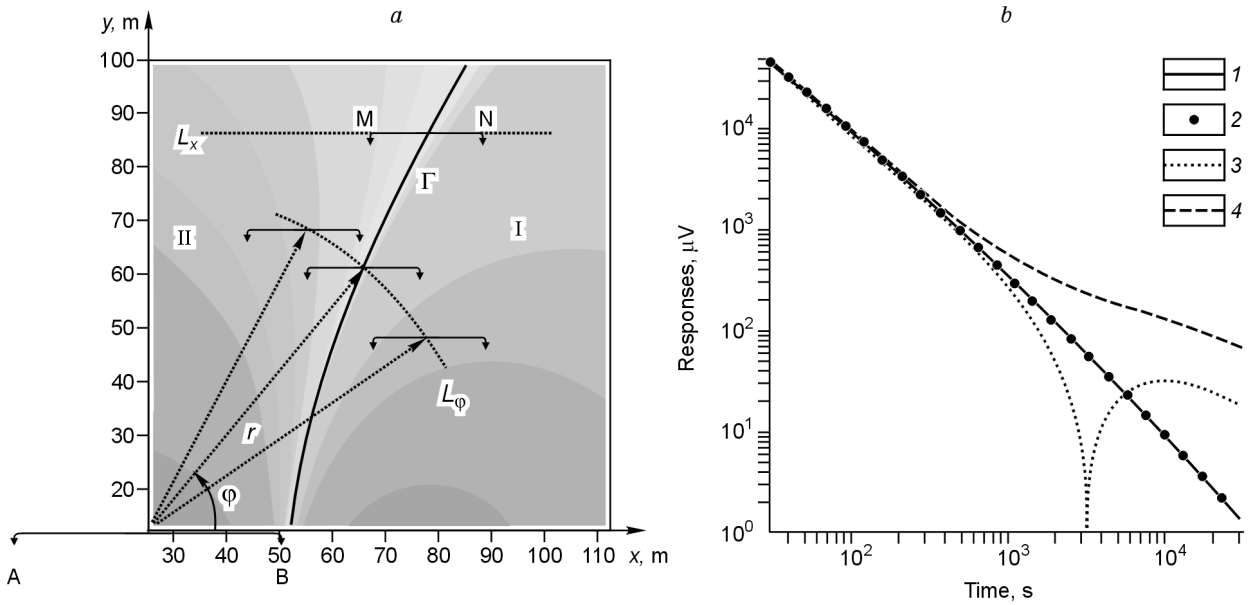

Fig. 4. Galvanic transient responses of a polarizable earth: *a* — positive signal (I) and sign reversal (II) zones separated by line B, for polarizable earth with ρ = 100 Ohm·m, η = 0.05, τ = 0.1 s, *c* = 0.5; *b* — data from a point along Γ: *1* — IP-free; *2–4* — IP-affected, for deviations from Γ of +0.5° (*3*) and –0.5° (*4*).

magnetic fields and their surface patterns, and showed a low sensitivity of the magnetic field components and a high sensitivity of the electric components. The current-parallel component turned out to be of special practical interest (see below).

Inversion of transients measured by an AB-MN array for various models of a layered polarizable earth resulted in a particular late-time pattern: There were two zones corresponding to positive and negative signals and, moreover, the boundary (Γ) between the zones passed through the points where IP effects were weak on the ground surface. This sign-reversal pattern is clearly seen in responses of a polarizable half-space with ρ = 100 Ohm·m, η = 0.05, τ = 0.1 s, *c* = 0.5, at a fixed delay time (Fig. 4). Thus, knowing the position of the sign-reversal boundary, one can achieve a high inversion quality for a nonpolarizable conductor. We suggest two ways of finding this boundary.

1. The array spacing is held fixed and the direction of the transmitter axis to the receiver center is allowed to vary (Fig. 4, *a*) by moving the receiver center along the arc L_φ. The zones of weak IP effects are found by forward modeling for the locus of points that make the line Γ. The search of the coordinates is reduced in this case to minimization of the functional

$$\Phi_{L_\varphi}(r, \varphi) = \left\{ \frac{1}{N-1} \sum_{i=1}^{N} \left[\frac{f(m_0, r, \varphi) - f(m_\omega, r, \varphi)}{f(m_0, r, \varphi)} \right]^2 \right\}^{1/2}, \qquad (6)$$

where r, φ are the receiver polar coordinates, m_0 is the model of a nonpolarizable layered conductor, m_ω is the model of a polarizable layered conductor, $f(m_0, r, \varphi)$, $f(m_\omega, r, \varphi)$ are the forward solutions for the m_0 and m_ω models, respectively. The solutions are found as the function $\varphi_\Gamma(r) = \min\limits_{\varphi \in \left[0, \frac{\pi}{2}\right]} \Phi_{L_\varphi}(r, \varphi)$.

2. The receiver is moved parallel to the transmitter while its y coordinate is fixed along L_x (Fig. 4, *a*). Then, the minimization functional for the search of points along Γ is

$$\Phi_{L_x}(x, y) = \left\{ \frac{1}{N-1} \sum_{i=1}^{N} \left[\frac{f(m_0, x, y) - f(m_\omega, x, y)}{f(m_0, x, y)} \right]^2 \right\}^{1/2}, \qquad (7)$$

where x and y are the Cartesian coordinates of the receiver center. We search the coordinates of the point at which the MN receiver center crosses the sign-reversal boundary: $x_\Gamma(y) = \min\limits_{x \in (0, \infty)} \Phi_{L_x}(x, y)$.

The optimization problems for the two ways of finding the line of weak IP effects are theoretically equivalent but the second way is advantageous in the field practice. The reason is that the vicinity of the sought point is highly sensitive to minor deviations of the receiver from Γ, and it is much easier to lay out and measure a profile than to vary the azimuth checking it against exact system positioning. See Fig. 4, *b* for transients corresponding to zones of monotonous and reversed sign and a point on Γ, as well as a response from a nonpolarizable earth. The transients of the polarizable and nonpolarizable cases coincide (curves 1 and 2 in Fig. 4, *b*) when the receiver line follows the boundary Γ. The errors caused by a 5° departure from Γ are minor in the responses of a nonpolarizable half-space but notable for a polarizable earth (curves 3, 4, in Fig. 4, *b*). The same applies to laying out parallel transmitter-receiver lines. The configuration quality is critical in this case because any azimuth error or an

off-parallel position of the lines can cause inversion errors for polarizable-earth transients.

It is important to learn how much the optimal array configuration can reduce IP effects. This test is convenient with a field amenable to analytical expression. For a polarizable half-space, the transient response to removal of transmitter current is related to the frequency response via an integral Fourier transform, which can be written either in the complex form

$$E_{\parallel}(t) = \frac{1}{2\pi}\int_{-\infty}^{\infty} E_{\parallel}(\omega)e^{-i\omega t}\,\frac{d\omega}{-i\omega},$$

or as the sine (cosine) transformation

$$E_{\parallel}(t) = -\frac{2}{\pi}\int_{0}^{\infty} \mathrm{Im}\,[E_{\parallel}(\omega)]\,\frac{\cos\omega t}{\omega}\,d\omega = \frac{2}{\pi}\int_{0}^{\infty} \mathrm{Re}\,[E_{\parallel}(\omega)]\,\frac{\sin\omega t}{\omega}\,d\omega.$$

The frequency response $E_{\parallel}(\omega)$ is

$$E_{\parallel}(\omega) = \frac{I_x\,dl}{2\pi r^3}\,[(3\cos^2\varphi - 2) + (1 + kr)e^{-kr}]\rho(\omega),$$

where $k^2 = -i\omega\mu_0/\rho(\omega) = -i\omega\mu_0\sigma(\omega)$. The $E_{\parallel}(t)$ component is obviously independent of azimuth in isotropic nonpolarizable conductors, but not in a polarizable earth. In order to see how the angle between the transmitter moment and the direction to the receiver influences the system's IP sensitivity, we consider a low-frequency decomposition for the imaginary part of $E_{\parallel}(\omega)$:

$$\mathrm{Im}\,[E_{\parallel}(\omega)]|_{kr \ll 1} \approx \mathrm{Im}\left[\frac{Idl}{2\pi r^3}\left(3\cos^2\varphi - 1 - \frac{k^2r^2}{2}\right)\rho(\omega)\right] =$$

$$\left\{\frac{I_x\,dl}{2\pi r^3}\,(3\cos^2\varphi - 1)\,\mathrm{Im}\,[\rho(\omega)]\right\} -$$

$$\frac{I_x\,dl\omega\mu_0 r^2}{4\pi r^3}\,\mathrm{Re}\,[\rho(\omega)]\,\mathrm{Im}\,[\rho(\omega)]. \qquad (8)$$

The azimuth dependence is provided by the braced first term in (8). Solving the equation $3\cos^2\varphi - 1 = 0$ gives that the IP effect is the minimum at $\varphi = \arccos\frac{1}{\sqrt{3}} \approx 54.736°$. Thus, the equation for the transient response of a polarizable earth can be divided into two parts describing the polarization and induction components:

$$E_{\parallel}^{\mathrm{IP}}(t) = \frac{I_x\,dl}{4\pi^2 r^3}\int_{-\infty}^{\infty}(3\cos^2\varphi - 1)\rho(\omega)\,\frac{e^{-i\omega t}}{-i\omega}\,d\omega, \qquad (9)$$

$$E_{\parallel}^{\mathrm{Ind}}(t) = \frac{I_x\,dl}{4\pi^2 r^3}\int_{-\infty}^{\infty}[-1 + (1 + kr)e^{-kr}]\rho(\omega)\,\frac{e^{-i\omega t}}{-i\omega}\,d\omega. \qquad (10)$$

Inasmuch as the equation for $E_{\parallel}^{\mathrm{Ind}}(t)$ includes complex resistivity, the separation into the polarization and inductive components is incomplete. However, it is the best approximation of the response from a nonpolarizable conductor being represented by an induction component only. This property of IP-affected transients is controlled by the relative transmitter-receiver position rather than by the Cole-Cole parameters of the half-space. In a real measurement system, the position of points along the line of minimum IP effects (Γ) depends on the array size. Figure 5 demonstrates inversion of dipole-dipole (curves 1 and 3) and line-line (curves 2, 4; AB = 100 m, MN = 50 m) data in polar (Fig. 5, *a*) and Cartesian (Fig. 5, *b*) coordinates, for two reference models. The models were, respectively, of a uniform polarizable half-space with $\rho = 100$ Ohm·m, $\eta = 0.05$, $\tau = 0.1$ s, and $c = 0.5$ (curves 1, 2) and a polarizable half-space overlain by a 50 m thick nonpolarizable conductor with $\rho = 100$ Ohm·m (curves 3, 4).

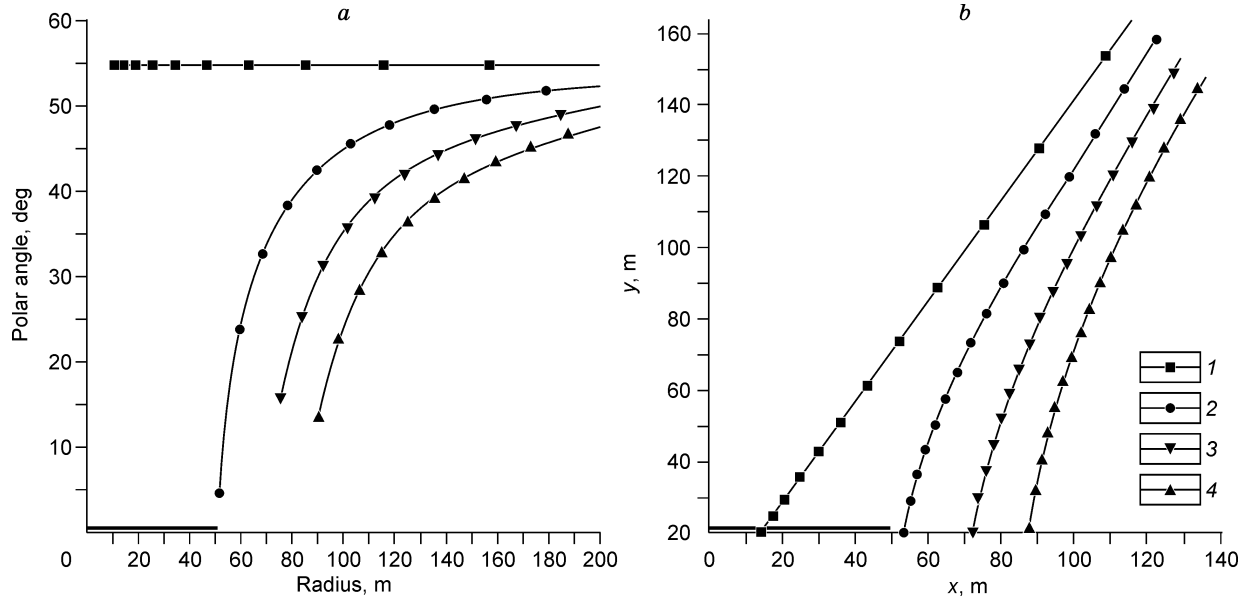

Fig. 5. Inversion results. Boundaries between monotonous and sign reversal zones in polar (*a*) and Cartesian (*b*) coordinates. *1*, *3* — dipole-dipole array; *2*, *4* — line-line array. Reference models: *1*, *2* — polarizable earth; *3*, *4* — polarizable earth beneath a nonpolarizable conductor.

We solved (6) to locate the points of the low-IP line and found out that the position of the line B depended on both the array size and the model parameters, especially the nonpolarizable conductor thickness in the two-layer model (Fig. 5). The computed locations of the low-IP points highlighted some limitations of the method. For instance, the inverted transient responses at a boundary point of two polarizable layers with different parameters showed a bad fit to the reference model of a nonpolarizable subsurface. Nevertheless, the sign-reversal boundary is better for constraining the parameters of the nonpolarizable reference model than the parallel or equatorial position of the receiver.

The method is especially good for the cases of
— a polarizable half-space;
— a polarizable layer above a conductor;
— a three-layer earth with a polarizable middle layer;
— a polarizable layer beneath a conductor.

Field examples

The theoretical results were tested in field experiments at two sites in the vicinity of Novosibirsk.

Site 1 is located near a clay quarry 10 km northeast of Novosibirsk in the left side of the Kamenka River (right tributary of the Ob'), 12 km upstream of its mouth. The local geology (Vasyutinskaya and Mikhailovskii, 1963) comprises a Late Devonian basement of sandstone, siltstone, clay and silty-clay shale, and limestone covered with a 10–20 m thick weathering mantle, and quite thin sediments. The basal sedimentary layer (Upper Neogene to Lower Pleistocene) is composed of 10–20 m thick limnic-bog and slope-wash clay and loam overlain by alluvial-limnic sand, loamy sand, and sandy loam and subaerial loam with interbeds of Quaternary slope-wash sand and loamy sand; the thickness of Quaternary layers varies from 15 to 40 m depending on topography.

Site 2 occurs 8 km southeast of Verkh-Irmen' Village (Novosibirsk Region, Ordynskoe District), 200 m far from the Novosibirsk water reservoir (left side), on the second terrace. The geology of the area (Misyuk and Kazennov, 1979) consists of a Paleozoic basement of Early Carboniferous sandstone, siltstone, mudstone, and silty-clay shale overlain by a ~60 m thick sedimentary section of about 10 m alluvial sand below 15 m of Late Quaternary alluvial pebble and sand, which make the base of the second terrace, followed upsection by 30–40 m of alluvial loamy sand and sandy loam, loessy loam, and slope-wash loamy sand.

The measurements were performed by a coincident-loop (100×100 m), loop-in-loop (100×100 m transmitter, 50×50 m receiver) and parallel galvanic (AB = 100 m, NM = 50 m) systems. The inversion quality was evaluated according to the rms error found as

$$\mathrm{rms} = \left\{ \frac{1}{N-1} \sum_{i=1}^{N} \left[\frac{f^{\mathrm{field}}(t_i) - f^{\mathrm{model}}(t_i)}{f^{\mathrm{field}}(t_i)} \right]^2 \right\}^{\frac{1}{2}},$$

where $f^{\mathrm{field}}(t)$ and $f^{\mathrm{model}}(t)$ are the field and synthetic responses, respectively, and N is count.

Clay Quarry. First we measured loop-in-loop responses and obtained a resistivity pattern for layered conductors (Fig. 6, *a*). Then we applied the equatorial current array with a spacing of 25 m and an azimuth of 90°. The model we obtained from inductive data (Table 3) was used to specify dc resistivity (ρ_0) and layer thicknesses. Inversion of these data, with regard to IP effects, at fixed ρ_0 and h, yielded a model of the subsurface with a polarizing second layer (see Table 4 for the model parameters and Fig. 6, *b* for the curves).

Inversion in which only polarization parameters were allowed to vary (Table 4) and the resistivity was fixed was of a worse quality (in terms of rms error). The error was much lower when both resistivity and polarization parameters were allowed to vary (Table 5, Fig. 6, *c*).

Inversion of inductive data gave a longitudinal resistivity of the second layer of $\rho_{2,i} = 16$ Ohm·m. The effective resistivity inferred from galvanic data was $\rho_{2,\mathrm{eff}} \sqrt{\rho_{2,i}\rho_{2,n}} = 40$ Ohm·m, which reflected the sensitivity of the system to both longitudinal and transverse resistivity. The corresponding anisotropy was estimated at $\lambda_2 = \rho_{2,\mathrm{eff}}/\rho_{2,i} = \sqrt{\rho_{2,n}/\rho_{2,i}} = 2.5$.

The discrepancy between the models obtained through inversion of inductive and galvanic data is evidence that the systems differ in their sensitivity to resistivity anisotropy and the spatial heterogeneity of the subsurface.

Verkh-Irmen' Village. First we performed coincident and loop-in-loop measurements, and then processed the inductive data to obtain the models shown in Fig. 6, *d*, *e*.

The results agree with the available knowledge of regional geology (40 to 300 m thick sediments over a high-resistivity basement). The models from Table 6 were used as an initial approximation in inversion of the galvanic responses (Fig. 6, *e*) measured with a spacing of 75 m and an azimuth of 30, which gave the model of Table 7.

Table 3
Inversion of induction array data without regard for IP effects (Clay Quarry), rms error = 0.04

Layer	ρ, Ohm·m	*h*, m
1	49	4
2	16	44
3	1700	∞

Table 4
Inversion of IP-affected induction array data (Clay Quarry), rms error = 0.3

Layer	ρ, Ohm·m	*h*, m	η	τ, s	*c*
1	49	4	—	—	—
2	16	44	0.073	$7.6 \cdot 10^{-4}$	0.53
3	1700	∞	—	—	—

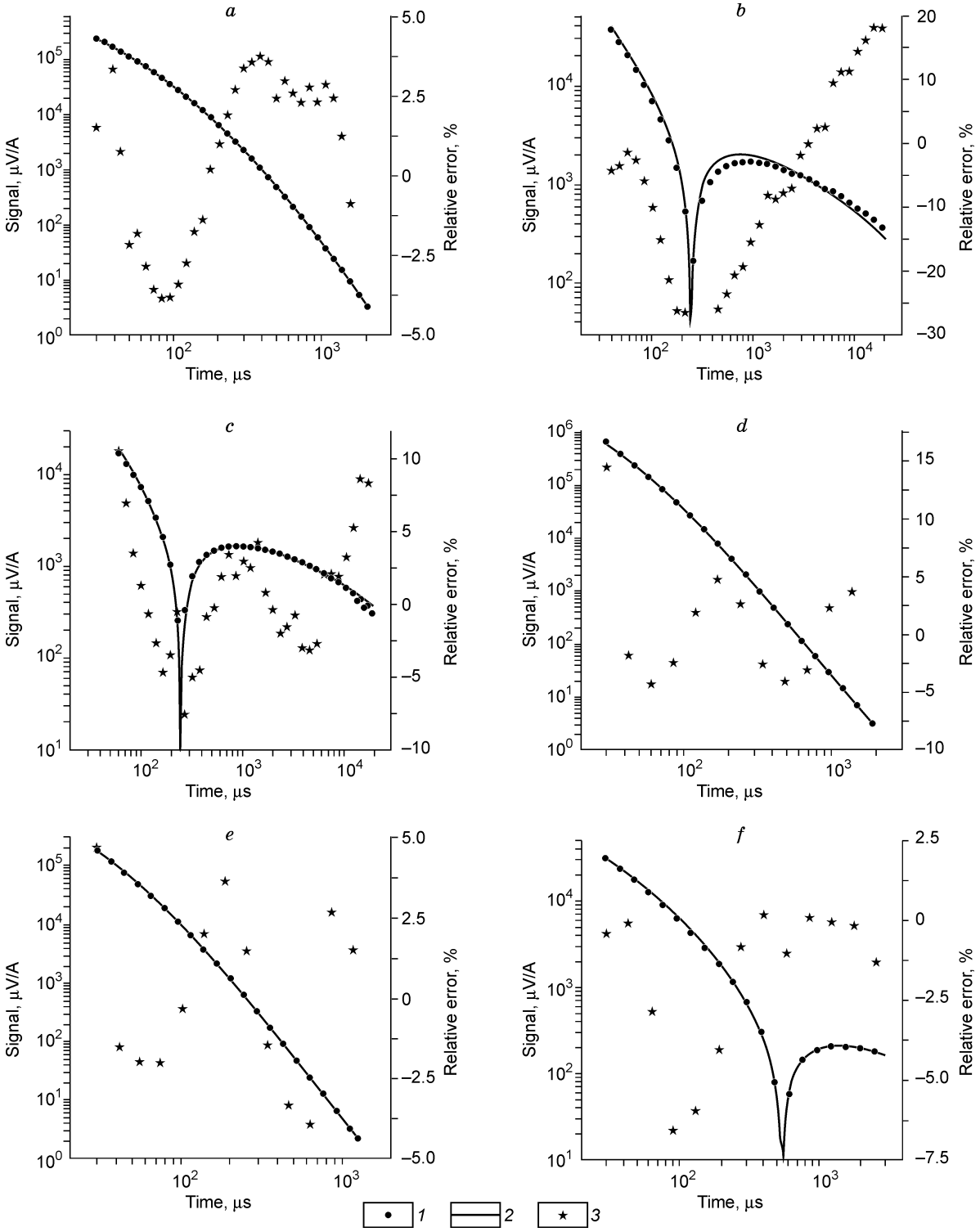

Fig. 6. Inductive and galvanic data inversion, for *a*, *d*, *e* — (ρ, *h*); *b* — (η, τ, *c*); *c*, *f* — (ρ, η, τ, *c*). *a*, *e* — loop-in-loop; *b*, *c* — equatorial galvanic array; *d* — coincident loop; *f* — parallel galvanic array (φ = 30°). *1* — field transient, *2* — synthetic transient; *3* — relative error.

Note that the positions of layer boundaries remained remarkably invariable in the separate inversion of inductive and galvanic data.

The following tests concerned the efficiency of parallel galvanic measurements in finding the line of low IP effects. See Fig. 7 for the responses obtained at different azimuths. The field and computed data were quite consistent. The pattern of the current-parallel electric component on the ground surface showed prominent zones of monotony and sign reversal and, hence, a boundary between the two zones where the IP effects were reduced to minimum.

Clay Quarry. Measurements at the Clay Quarry site by a line-line galvanic array (AB = 100 m, MN = 50 m) at a spacing of 77 m and azimuths of 60°, 20°, 45°, and 31°

Table 5
Inversion of IP-affected equatorial galvanic array (Clay Quarry), rms error = 0.07

Layer	ρ, Ohm·m	*h*, m	η	τ, s	*c*
1	49	4	—	—	—
2	40	44	0.014	$6.2 \cdot 10^{-3}$	0.63
3	1700	∞	—	—	—

Table 6
Inversion of induction array (Verkh-Irmen' Village)

Layer	Coincident loop, rms = 0.09		Loop-in-loop, rms error = 0.04	
	ρ, Ohm·m	*h*, m	ρ, Ohm·m	*h*, m,
1	35	22	36	22
2	133	22	110	22
3	48	22	60	22
4	3000	∞	3000	∞

Table 7
Inversion of parallel galvanic array (Verkh-Irmen' Village), rms error = 0.03

Layer	ρ, Ohm·m	*h*, m	η	τ, s	*c*
1	67	23	0.044	$1.0 \cdot 10^{-5}$	0.5
2	230	22	—	—	—
3	63	23	0.058	$1.4 \cdot 10^{-3}$	0.52
4	4800	*ind*	—	—	—

confirmed the theoretically predicted azimuth dependence of responses from a polarizable earth. Judging by the geometry of the transients, the IP effect was the lowest at 31°.

That result was reproduced in the inversion, to a good accuracy. See Table 8 for the fitting results and the model of a polarizable earth, and Fig. 8, *a* for the respective measured and computed transients and the rms errors.

The inversion of IP-affected data using a starting model of a nonpolarizable conductor (Table 8) allowed us to process the measurements at azimuths 45°, 20°, and 31° within the limits of a single model (Table 9). The corresponding computed and measured transients and their rms errors are shown in Fig. 8, *b*, *c*.

Verkh-Irmen' Village. In order to find the points where IP effects were the lowest, we applied soundings by a parallel galvanic array with a fixed spacing of 75 m for azimuths 45°, 20°, 30°, 25°, 27°, 29°, 28°, 28.5°, and 28.25°. We inverted the transients (Fig. 8, *d*) and arrived at the model of a nonpo-

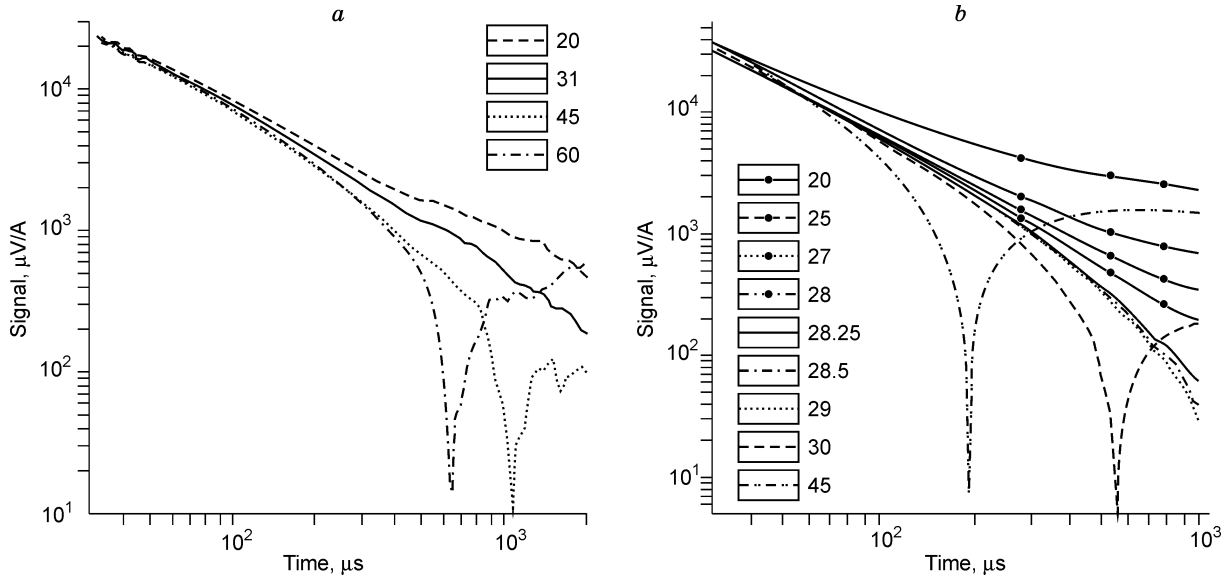

Fig. 7. Field transient responses. Symbols of curves are keyed according to azimuth. *a* — Clay Quarry; *b* — Verkh-Irmen' Village.

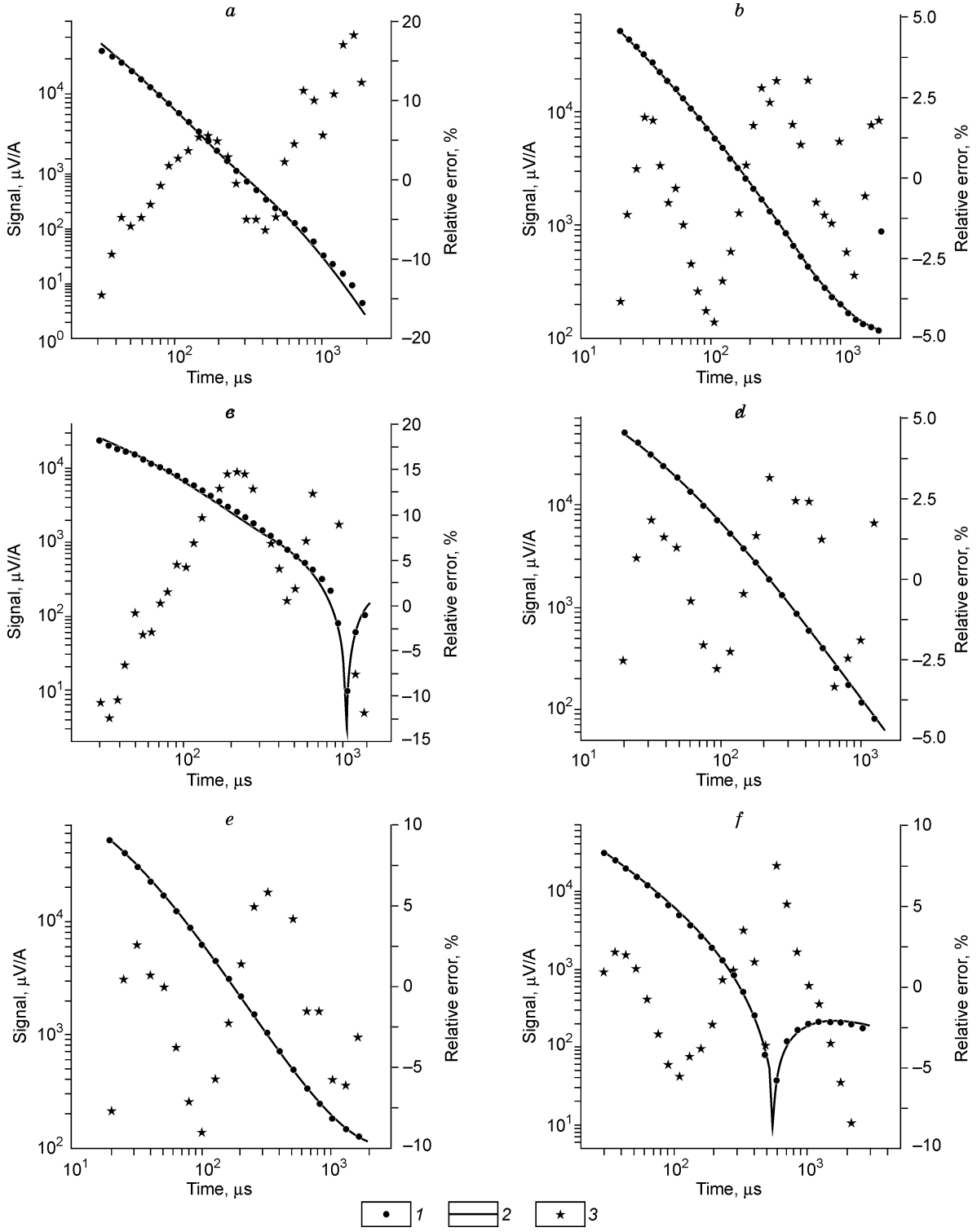

Fig. 8. Inversion of galvanic array, for different azimuths: *a* — 31°, *b* — 20°, *c* — 45°, *d* — 28.25°, *e* — 28°, *f* — 30°. Other symbols same as in Fig. 6.

larizable conductor as in Table 10, assuming that the line with the azimuth 28.25° centered at the point of the weakest IP effects.

Table 11 presents a layered polarizable earth model which agrees quite well with the data obtained at 28° and 30° (the respective curves are in Fig. 8, *e*, *f*).

Therefore, we may conclude that the tests were successful: we found the best configuration of the receiver line to minimize IP effects in transients, which is critical for reliable reconstruction of subsurface parameters. The field tests confirmed the theoretical predictions, though they were run in different geoelectrical settings.

Table 8
Inversion of data for azimuth corresponding to minimum IP effects (Clay Quarry), rms error = 0.08

Layer	ρ, Ohm·m	*h*, m
1	44	23.5
2	10	55.6
3	1700	∞

Table 9
Inversion of IP-affected data (Clay Quarry), rms error = 0.09

Layer	ρ, Ohm·m	*h*, m	η	τ, s	*c*
1	44	23.5	—	—	—
2	10	55.6	0.1	0.025	0.49
3	1700	∞	—	—	—

Table 10
Inversion of data from low-IP point (Verkh-Irmen' Village), rms error = 0.03

Layer	ρ, Ohm·m	*h*, m
1	73	22
2	125	19
3	66.5	21
4	5000	∞

Table 11
Joint inversion of IP-affected galvanic array (Verkh-Irmen' Village), rms error = 0.04

Layer	ρ, Ohm·m	*h*, m	η	τ, s	*c*
1	73	22	0.05	$1.0 \cdot 10^{-2}$	0.37
2	125	19	—	—	—
3	66.5	21	0.11	$4.4 \cdot 10^{-3}$	0.6
4	5000	∞	—	—	—

Conclusions

1. There exists a receiver configuration in parallel galvanic arrays, for each fixed array spacing, which reduces IP effects in transients. Thus, inversion is possible due to spatial separation of the polarization and induction components of transients.

2. The method is highly sensitive to the array geometry (transmitter and receiver size and relative position).

3. The use of current pulses of different durations is an additional way to gain useful information in galvanic measurements of a polarizable subsurface.

4. A way to improve the quality of galvanic data inversion is to use a starting model of a nonpolarizable conductor derived from inductive data.

We wish to thank I.D. Zol'nikov from the Institute of Geology and Mineralogy (Novosibirsk) for providing data on local geology, N.O. Kozhevnikov from the Institute of Petroleum Geology and Geophysics (Novosibirsk) for discussions, and A.E. Plotnikov from the SPE "Looch" for aid in the field.

References

Davydycheva, S., Rykhlinskii, N., Legeido, P., 2006. Electrical-prospecting method for hydrocarbon search using the induced-polarization effect. Geophysics 71 (4) G179–G189.

Epov, M.I., Nevedrova, N.N., Antonov, E.Yu., 2006. A way to take into account distortions in field TEM curves from active seismic areas. Geofizicheskii Vestnik 6, 8–14.

Gennadinik, B.I., 1967. On the nature of induced polarization in ion-conducting rocks. Izv. Vuzov. Geologiya i Razvedka 12, 110–117.

Gill, Ph. E., Myurray, W., Wright, M., 1981. Practical Optimization. Academic Press, New York.

Gubatenko, V.P., 1991. The Maxwell-Wagner effect in electrical prospecting. Izv. AN SSSR. Fizika Zemli 4, 88–98.

Hohmann, G.W., Kintzinger, P.R., Van Voorrhis, G.D., Ward, S.H., 1970. Evaluation of the measurement of induced electrical polarization with an inductive system. Geophysics 35 (5), 901–915.

Komarov, V.A., 1972. Induced Polarization Method of Electrical Prospecting [in Russian]. Nauka, Leningrad.

Kormil'tsev, V.V., 1980. Transient Processes in Induced Polarization. Theory and Geophysical Applications [in Russian]. Nauka, Moscow.

Kozhevnikov, N.O., Antonov, E.Yu., 2006. Fast decaying IP in frozen unconsolidated rocks and potentialities of its use in the permafrost-related TEM studies. Geophys. Prospect. 54 (4), 383–397.

Kozhevnikov, N.O., Antonov, E.Yu., 2007. Inversion of IP-affected TEM data: A numerical experiment with a model of a uniform polarizing half-space. Geofizika 1, 42–50.

Lee, T., 1981. Transient electromagnetic response of a polarizable ground. Geophysics 46 (7), 1037–1041.

Legeido, P.Yu., Mandel'baum, M.M., Rykhlinskii, N.I., 1990. Application of differentially adjusted electric exploration of the Nepa Dome. Geologiya i Geofizika (Soviet Geology and Geophysics) 31(4), 86–91.

Mandel'baum, M.M., Puzyrev, N.N., Rykhlinskii, N.I., Trofimuk, A.A., Surkov, B.C., 1988. Direct Petroleum Prospecting by Geophysical Methods [in Russian]. Nauka, Moscow.

Misyuk, V.A., Kazennov, A.I., 1979. Geological map of the USSR. Scale 1:200 000, ser. Kuzbas, Sheet N-44-XVII. Explanatory Note [in Russian]. Nedra, Moscow.

Nelder, J.A., Mead, R., 1965. A simplex method for function minimization. Computer Journal 7, 308–313.

Nevedrova, N.N., Antonov, E.Yu., 2004. Structure and geodynamics of the Chuya basin, Gorny Altai, from electromagnetic data, in: Shitov A.V. (Ed.), The Altai (Chuya) Earthquake: Predictions, Parameters, and Consequences [in Russian]. Izd. GAGU, Gorno-Altaisk, pp. 37–47.

Pelton, W.H., Ward, S.H., Hallof, P.G., Still, W.R., Nelson, P.H., 1978. Mineral discrimination and removal inductive coupling with multifrequency IP. Geophysics 43 (3), 588–609.

Postel'nikov, A.F., 1964. The nature and mechanism of induced polarization in samples of conductive rocks. Transactions, Central Research Mining Institute, Issue 59, pp. 153–164, Nedra, Moscow.

Rykhlinskii, N.I., Mandel'baum, M.M., Vashchenko, V.A., Alaev, N.V., 1970. Application of divergent logging in petroleum wells, in: V.S. Surkov (Ed.), Prospecting Geophysics: State of the Art and Challenges [in Russian]. Nedra, Moscow, pp. 223–227.

Sheinmann, S.M., 1969. The Theory of Electrical Prospecting: Modern Physical Background [in Russian]. Nedra, Leningrad.

Tabarovskii, L.A., 1975. Method of Integral Equations: Geoelectrical Applications [in Russian]. Nauka, Novosibirsk.

Tabarovskii, L.A., 1979. Transverse electric and transverse magnetic fields in layered media, in: Yu.N. Antonov (Ed.), Electromagnetic Logging Methods [in Russian]. Nauka, Novosibirsk, pp. 225–233.

Vasyutinskaya, T.F., Mikhailovskii, D.V., 1963. Geological map of the USSR. Scale 1:200 000, ser. Kuzbas, Sheet N-44-XII. Explanatory Note [in Russian]. Gosgeoltekhizdat, Moscow.

Yeltsov, I.N., Epov, M.I., Antonov, E.Yu., 1999. Inversion of inductive soundings for frequency dependence of resistivity. Geofizika 2, 65–67.

Yeltsov, I.N., Epov, M.I., Antonov, E.Yu., 2002. Reconstruction of Cole-Cole parameters from IP induction sounding data. J. Balkan Geophys. Soc. 5 (1), 15–20.

Editorial responsibility: M.I. Epov